Medical Physics
The International Journal of Medical Physics Research and Practice

WAXS fat subtraction model to estimate differential linear scattering coefficients of fatless breast tissue: Phantom materials evaluation

Robert Y. Tang, Curtis Laamanen, Nancy McDonald, and Robert J. LeClair

Citation: Medical Physics **41**, 053501 (2014); doi: 10.1118/1.4870982
View online: http://dx.doi.org/10.1118/1.4870982
View Table of Contents: http://scitation.aip.org/content/aapm/journal/medphys/41/5?ver=pdfcov
Published by the American Association of Physicists in Medicine

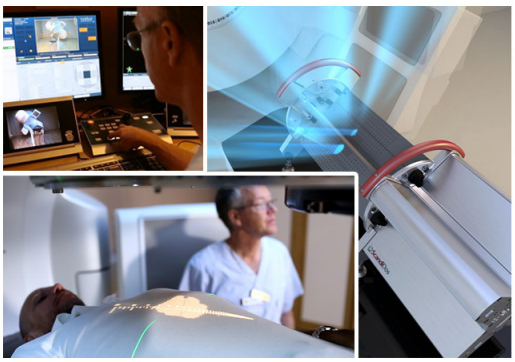

WAXS fat subtraction model to estimate differential linear scattering coefficients of fatless breast tissue: Phantom materials evaluation

Robert Y. Tang[a)]
Biomolecular Sciences Program, Laurentian University, 935 Ramsey Lake Road, Sudbury, Ontario P3E 2C6, Canada

Curtis Laamanen[b)] and Nancy McDonald[c)]
Department of Physics, Laurentian University, 935 Ramsey Lake Road, Sudbury, Ontario P3E 2C6, Canada

Robert J. LeClair[d)]
Department of Physics, Laurentian University, 935 Ramsey Lake Road, Sudbury, Ontario P3E 2C6, Canada and Biomolecular Sciences Program, Laurentian University, 935 Ramsey Lake Road, Sudbury, Ontario P3E 2C6, Canada

(Received 1 August 2013; revised 25 March 2014; accepted for publication 29 March 2014; published 16 April 2014)

Purpose: Develop a method to subtract fat tissue contributions to wide-angle x-ray scatter (WAXS) signals of breast biopsies in order to estimate the differential linear scattering coefficients μ_s of fatless tissue. Cancerous and fibroglandular tissue can then be compared independent of fat content. In this work phantom materials with known compositions were used to test the efficacy of the WAXS subtraction model.

Methods: Each sample 5 mm in diameter and 5 mm thick was interrogated by a 50 kV 2.7 mm diameter beam for 3 min. A 25 mm^2 by 1 mm thick CdTe detector allowed measurements of a portion of the $\theta = 6^\circ$ scattered field. A scatter technique provided means to estimate the incident spectrum $N_0(E)$ needed in the calculations of $\mu_s[x(E, \theta)]$ where x is the momentum transfer argument. Values of $\overline{\mu}_s$ for composite phantoms consisting of three plastic layers were estimated and compared to the values obtained via the sum $\overline{\mu}_s^{\sum}(x) = \nu_1\mu_{s1}(x) + \nu_2\mu_{s2}(x) + \nu_3\mu_{s3}(x)$, where ν_i is the fractional volume of the ith plastic component. Water, polystyrene, and a volume mixture of 0.6 water + 0.4 polystyrene labelled as fibphan were chosen to mimic cancer, fat, and fibroglandular tissue, respectively. A WAXS subtraction model was used to remove the polystyrene signal from tissue composite phantoms so that the μ_s of water and fibphan could be estimated. Although the composite samples were layered, simulations were performed to test the models under nonlayered conditions.

Results: The well known μ_s signal of water was reproduced effectively between $0.5 < x < 1.6$ nm^{-1}. The $\overline{\mu}_s$ obtained for the heterogeneous samples agreed with $\overline{\mu}_s^{\sum}$. Polystyrene signals were subtracted successfully from composite phantoms. The simulations validated the usefulness of the WAXS models for nonlayered biopsies.

Conclusions: The methodology to measure μ_s of homogeneous samples was quantitatively accurate. Simple WAXS models predicted the probabilities for specific x-ray scattering to occur from heterogeneous biopsies. The fat subtraction model can allow μ_s signals of breast cancer and fibroglandular tissue to be compared without the effects of fat provided there is an independent measurement of the fat volume fraction ν_f. Future work will consist of devising a quantitative x-ray digital imaging method to estimate ν_f in *ex vivo* breast samples. © *2014 American Association of Physicists in Medicine*. [http://dx.doi.org/10.1118/1.4870982]

Key words: wide-angle x-ray scatter (WAXS), differential linear scattering coefficients, breast tissue, fat, biopsies, CdTe

1. INTRODUCTION

Diagnosing breast cancer is a multistep process involving clinical examination and/or mammography to detect lesions, surgery to remove tissue, and histology to analyse several slices of the tissue. The slices chosen are based upon a meticulous anatomic examination by a pathologist.[1] Khaddage *et al.*[2] studied intraoperative techniques used in sentinel lymph node breast biopsies and found it is important to analyse a greater proportion of sectioned tissue to minimize sampling errors.

Wide-angle x-ray scatter (WAXS) methods are being used to characterize breast tissue.[3–12] An x-ray scatter method can potentially become a complementary method to histology for determining whether a biopsy is malignant or benign. In this work, WAXS models for the purpose of analyzing breast tissue were devised and experimentally tested with phantom materials.

A pioneering WAXS work on 100 breast tissue samples was done by Kidane *et al.*[12] They extracted differential linear scattering coefficients (μ_s) of breast tissue via WAXS energy dispersive experiments performed at $\theta = 6^\circ$ using an 80 kV

beam and a HPGe detector. The composition of each sample was estimated by histological analysis of 5 μm sections. Their μ_s data for cancer obtained upon removal of the fibrous and fat components were quite different from fibroglandular tissue. The use of histology to estimate fat content is questionable because there is no guarantee the composition of the chosen slice is the same throughout the sample.

Griffiths *et al.*[9] performed imaging in order to obtain more detailed data on the composition of their breast tissue samples. They generated microCT transmission (30 kVp, Mo anode, pixellated amorphous silicon array) and diffraction (70 kVp, W anode, $\theta = 6^\circ$, HPGe detector) images of 19 samples. Diffraction images were generated using $x = 1.1$ and 1.5 nm^{-1} data where the momentum transfer variable x combines the dependence of scatter on angle (θ) and x-ray wavelength (λ). Images of 1 mm thick sections were segmented, coregistered, and compared to histology stains. Diffraction signatures as a function of x were acquired for the 1 mm thick tissue sections, two of which were estimated to be pure tumor and pure fat. The scatter signal at 1.1 nm^{-1} is lower than that at 1.5 nm^{-1} when a sample is predominantly tumor. The study concluded that the ratio of the signals at these two values of x can be used to characterize tissue.

From an x-ray perspective, normal breast tissue can be considered to consist of two main types: fat and fibroglandular tissue.[13] Fat tissue is loose connective tissue composed of fat cells whereas fibroglandular tissue has fibrous connective tissue and epithelial cells. In a previous work,[11] μ_s breast data were measured with a stationary W anode tube and a cadmium zinc telluride (CZT) energy dispersive system. Comparisons of μ_s between cancerous and fibroglandular tissue showed differences but results were not consistent. Biopsies are heterogeneous in nature and the presence of fat could have affected the results.

A WAXS model[11] for homogeneous samples was modified and extended to heterogeneous applications, with particular emphasis on its use to eliminate the effects of fat in WAXS signals. Consider a biopsy that contains fat with fractional volume ν_f and another material η. The experimental/analysis protocol to extract μ_s of material η is the following: (1) measure the scatter spectrum N_s of the biopsy, (2) calculate $\overline{\mu}_s$ for the composite sample, and then (3) subtract from it the contribution due to fat. The ν_f needs to be known to accomplish this task. In this paper breast biopsy phantoms were used and the amount of polystyrene which was chosen to approximate fat was known. Future work will examine a quantitative method to estimate ν_f in the samples. The WAXS models for practical uses with experimental data are now described.

2. WAXS MODELS

A semianalytic model[11,14–17] can be used to estimate the number of scattered photons from tissue samples with known scattering properties. Consider a pencil beam of x rays that irradiates a homogeneous sample of thickness d as shown in Fig. 1. Let $N_0(E)$ denote the number of incident x rays each of energy E. An energy dispersive photon counting detector is situated at a distance r and angle θ with respect to the sample

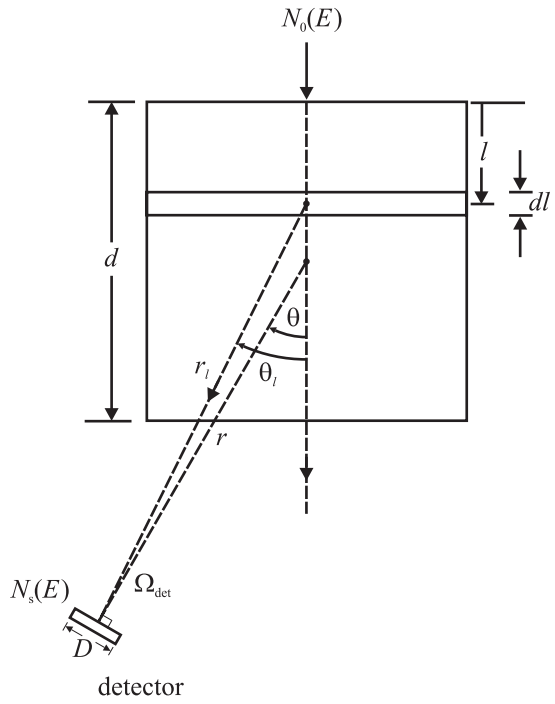

FIG. 1. Homogeneous model (not to scale).

center. The following expression can be used to estimate the number of scattered x rays originating in segment of thickness dl that reach the detector

$$dN_s(E,\theta) = \int_{\Omega_{det}} N_0(E) e^{-\mu(E)l} \mu_s(x_l) e^{-\mu(E)\frac{(d-l)}{\cos\theta_l}} d\Omega dl, \quad (1)$$

where $\mu(E)$ and $\mu_s(x_l)$ are the total linear attenuation and differential linear scattering coefficients of the sample, $x_l = \sin(\theta_l/2)/\lambda$, and the integration is over the solid angle subtended by the detector. The geometry chosen for the experiments ($r = 43$ cm, $d = 5$ mm, detector active diameter $D = 4.2$ mm) is such that over the thickness d, $\theta_l \approx \theta$ and μ_s can be considered to be a constant over the detector surface. With these approximations the expression for the total scatter from the sample becomes

$$N_s(E,\theta) = \frac{N_0(E)\mu_s[x(E,\theta)]\Omega_{det} e^{-\mu(E)\frac{d}{\cos\theta}}}{\mu(E)\left(1-\frac{1}{\cos\theta}\right)} \times \left[1 - e^{-\mu(E)d\left(1-\frac{1}{\cos\theta}\right)}\right], \quad (2)$$

where $\Omega_{det} = \pi D^2/(4r^2)$. This expression assumes: (i) all scattering occurs along the central vertical axis of the sample, (ii) the Compton wavelength shift is negligible, and (iii) multiple scatter is negligible. Rearrangement of Eq. (2) yields an expression for μ_s, namely,

$$\mu_s[x(E,\theta)] = \frac{N_s(E,\theta)}{N_0(E)\Omega_{det}} \times \frac{\mu(E)\left(1-\frac{1}{\cos\theta}\right)e^{\mu(E)\frac{d}{\cos\theta}}}{\left[1 - e^{-\mu(E)d\left(1-\frac{1}{\cos\theta}\right)}\right]}. \quad (3)$$

Given a measurement of $N_s(E, \theta)$, an estimate of $N_0(E)$, and μ values, the μ_s can be obtained for homogeneous samples.

For heterogeneous samples an approximation for μ_s denoted by $\overline{\mu}_s$ can be calculated from $N_s(E, \theta)$ provided the

amounts of each tissue type are known. For example, the $\overline{\mu}_s$ for a sample consisting of three tissue types can be approximated via Eq. (3) with $\mu(E)$ replaced by

$$\overline{\mu}(E) = \nu_1\mu_1(E) + \nu_2\mu_2(E) + \nu_3\mu_3(E), \quad (4)$$

where ν_i is the fractional volume of the ith tissue type. The calculation requires no knowledge of the locations of the tissue components within the sample. The $\overline{\mu}_s$ was compared to the sum

$$\overline{\mu}_s^{\sum} = \nu_1\mu_{s1} + \nu_2\mu_{s2} + \nu_3\mu_{s3}, \quad (5)$$

where μ_{si} were obtained via Eq. (3). The summation method is similar to that used by Kidane *et al.*[12] with the exception that ν was the fractional weight.

Consider a sample consisting of a material η and fat (f). Suppose the scatter spectrum $N_s(E,\theta)$ was measured and that the fractional volume of fat denoted by ν_f was known. The μ_s for material η can be approximated by

$$\mu_{sc}^{\eta}(E,\theta) = \left(\frac{N_s(E,\theta)}{N_0\Omega_{det}} \times \frac{\overline{\mu}(E)\left(1-\frac{1}{\cos\theta}\right)e^{\overline{\mu}(E)\frac{d}{\cos\theta}}}{\left[1-e^{-\overline{\mu}(E)d\left(1-\frac{1}{\cos\theta}\right)}\right]} - \nu_f\mu_s^f\right) \Big/ (1-\nu_f), \quad (6)$$

where $\overline{\mu} = (1-\nu_f)\mu_\eta + \nu_f\mu_f$ and the subscript "c" denotes that the μ_s was obtained via subtraction (correction) of fat.

3. METHOD

3.A. Samples

Samples of polystyrene (polyst), nylon, polymethyl methacrylate (PMMA), and polycarbonate (polyca) were used. The stoichiometric unit for each plastic are C_8H_8 (polyst), $C_6H_{11}NO$ (nylon), $C_5H_8O_2$ (PMMA), and $C_{16}H_{14}O_3$ (polyca).[18] The samples were machined to have 5 mm diameters and thicknesses ranging from 1 to 5 mm. Values of $\overline{\mu}_s$ were obtained for the following three-compartment phantoms: (A) 3 mm polyst (top) + 1 mm nylon (middle) + 1 mm PMMA (bottom), (B) 1 mm polyst + 3 mm nylon + 1 mm PMMA, and (C) 1 mm polyst + 1 mm nylon + 3 mm PMMA.

Figure 2 shows the $\mu_s(x)$ values (solid lines) for (a) adipose tissue (fat), (b) breast cancer, and (c) fibroglandular tissue acquired at $\theta = 6^\circ$ by Kidane *et al.*[12] Fat has a distinct μ_s peak at $x = 1.1$ nm^{-1} because of the preferred orientation of triacylglycerol molecules.[19] Inter-chain interactions of their hydrocarbon chains in a lateral two-chain packing is correlated to a d-spacing of 4.6 Å.[20] Polyst, a glassy polymer that has two broad Bragg peaks[21] approximates the fat signal. The first peak corresponds to interchain interferences (8.84 Å) where large phenyl groups prevent neighbouring chains from getting close to each other. The second peak is due to intramolecular interferences (4.67 Å) such as those between phenyl groups.[21] The μ_s of polyst was extracted from the diffraction data of Kosanetzky *et al.*[22] The water μ_s which approximates cancer [Fig. 2(b)] was calculated using coherent form factors F measured by Narten[23] and incoherent scattering functions (S) from Hubbell *et al.*[24] Figure 2(c) shows that a phantom called fibphan consisting of

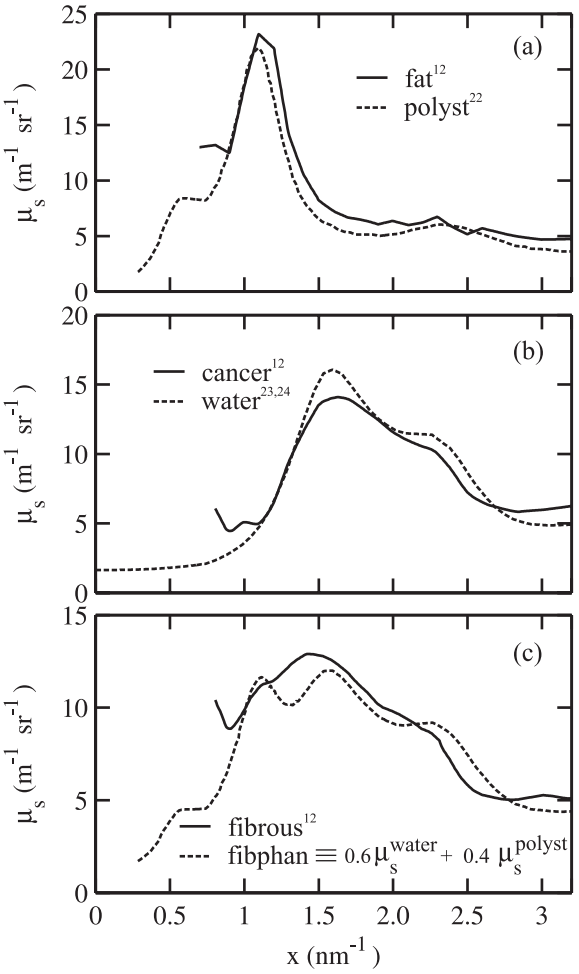

FIG. 2. (a)–(c) $\mu_s(x)$ data for three breast tissue types (Ref. 14), and corresponding phantoms: (a) fat/polyst, (b) cancer/water, and (c) fibrous/fibphan.

60% water and 40% polyst volumes behaves somewhat like fibroglandular tissue. This sample will be treated as homogeneous fibroglandular tissue but actually consists of two layers. The scattering coefficients for fibphan were calculated via $\mu_s^{fibphan} = 0.6 \times \mu_s^{water} + 0.4 \times \mu_s^{polyst}$. The scatter signal for breast fat is well known but those of cancer and fibrous tissue are not as well understood. For the latter two, Griffiths *et al.*[9] obtained different signals as compared to Kidane *et al.*[12] Here, the phantoms chosen will suffice to demonstrate the utility of the fat subtraction model.

μ values of plastics and breast phantoms were calculated using the sum rule[15] and cross section data of elements.[25] Johns and Yaffe[26] measured linear attenuation coefficients of breast tissue using a HPGe spectroscopy system. Over the energy range of interest, the average percent differences between μ values of the breast phantoms and tissues were: 6% for polyst vs fat, 9% water vs cancer, and 19% fibphan vs fibrous.

The estimation of $\mu_s(x)$ of a material via the subtraction model was demonstrated using the samples listed in Table I. The 2 mm water + 3 mm polyst composite was also treated as a 3.33 mm fibphan + 1.67 mm polyst composite. The polyst signals were subtracted from the N_s signals so as to evaluate Eq. (6) for water and fibphan.

TABLE I. Composite samples used to test the WAXS subtraction model.

Water (mm)	Polyst (mm)
4	1
3.5	1.5
3	2
2	3
1	4

3.B. WAXS Measurements

The WAXS system is housed in an x-ray cabinet (Model 43855C, Faxitron X-Ray Corporation, Chicago IL). It consists of a stationary anode tungsten tube, a MAGNA 1cc parallel plate chamber (Standard Imaging Inc., Middleton WI), pinhole apertures, translation and rotation stages (Unislide Model, Velmex Inc., Bloomfield NY), and a cadmium telluride (CdTe) 25 mm^2 by 1 mm thick crystal (XR-100T-CdTe, Amptek Inc., Bedford MA). Room temperature semiconductor detectors (e.g., CZT, CdTe) are known to have problems with fluorescence escape and hole tailing.[27] A response function model[27] could be devised but was omitted. In Ref. 11 the μ_s curves obtained for water with and without detector corrections were similar.

Figure 3 shows a schematic of the scatter geometry. A 50 kV beam 2.7 mm in diameter at the surface of the sample and of 3 min duration yielded an entrance exposure of 0.12 C/kg. The ion chamber provided a means to correct for tube output fluctuations. Scatter signals from the cylindrical shaped region of interest (ROI) were measured at 6° with the CdTe crystal which was collimated by a 4.2 mm diameter Pb aperture.

In previous work[11] the effects of air scatter were neglected and N_0 was estimated via direct measurements with a small aperture on a CZT detector. Results of μ_s for water

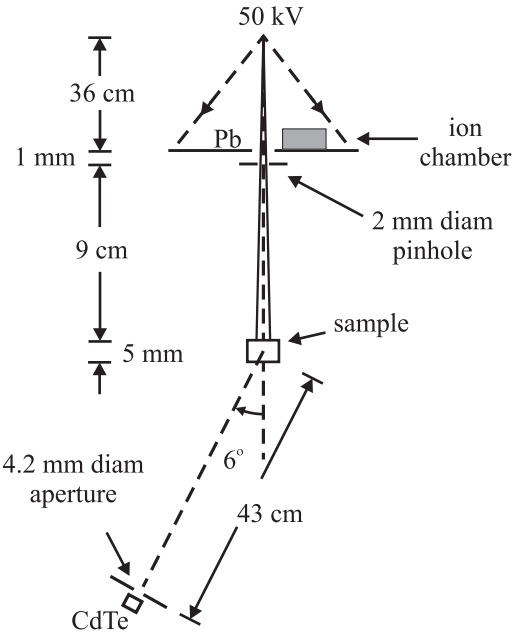

FIG. 3. Scatter geometry for experiments (not to scale).

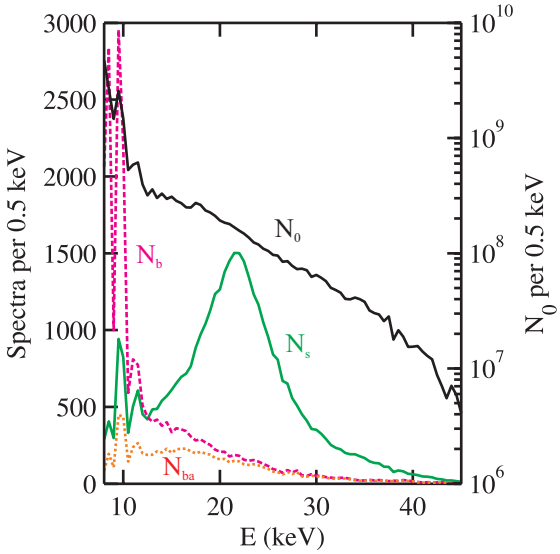

FIG. 4. Polyca scatter and background spectra measured at 6° and attenuated background and N_0 estimate.

obtained at $\theta = 6°$ did not match for $x < 1.3$ nm^{-1} the gold standard data.[23,24] In this work a different approach was used.

Figure 4 shows two measured spectra and two processed spectra. The measured ones are the scatter N_s spectrum (220 counts/s) for a 5 mm thick polyca sample and a background N_b spectrum (125 counts/s) which was obtained when the sample was removed. The energy range from 8 to 45 keV was chosen for analysis. The sharp peaks at low energies were due to L-fluorescence from the tungsten anode. The background was due to air scatter which originates from where the direct $\theta = 0°$ beam was present. When a homogeneous sample is analysed, the amount of air scatter reaching the detector will be reduced to $N_b(E)e^{-\mu(E)d}$ where μ is the attenuation coefficient of the sample. The N_{ba} spectrum shown in Fig. 4 was obtained for a 5 mm thick polyca sample. Corresponding attenuated background spectra were subtracted from all N_s spectra. The detector dead times for all spectra were negligible (less than 1%). In the applications of WAXS models, only statistical noise was included in the calculations of the error bars.

In order to extract accurate μ_s values a good N_0 estimate is required. A direct measurement of N_0 with small apertures requires precise alignment of the system. A more forgiving method is to use an x-ray scatter technique.[28] A rearrangement of Eq. (2) yields an expression for N_0 which can be evaluated by measuring the N_s spectrum of a sample with a known μ_s signal. The use of $N_s(E, \theta = 6°)$ from polyca and μ_s from Ref. 22 provided the N_0 estimate shown in Fig. 4 (right y-axis). A drawback to this method is its dependancy on an external scatter coefficient measurement. However, an analysis could have be done without N_0 if μ_s coefficients were not sought.

3.C. Simulations

Simulations using the same geometry as the WAXS measurements were done to test the models. The scattered number of photons $N_s(E, \theta = 6°)$ was computed for a 2.7 mm

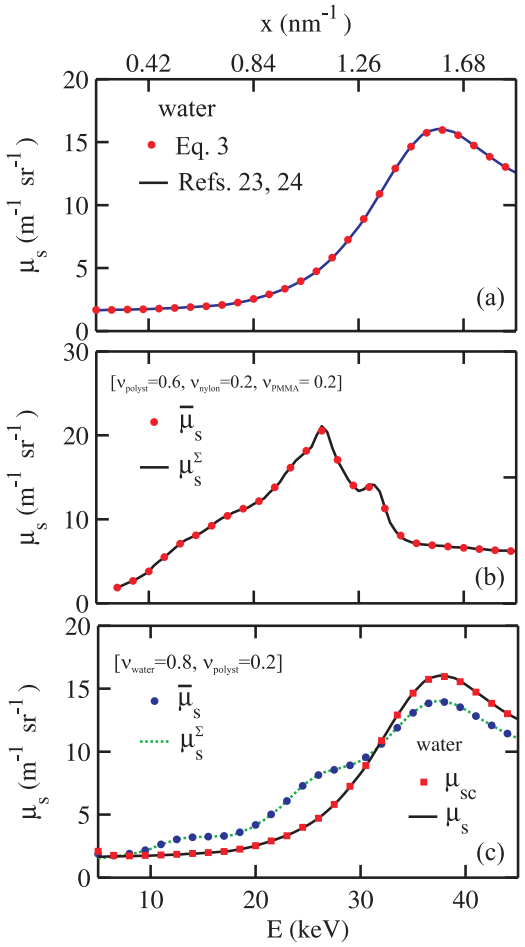

FIG. 5. Testing models with simulations: (a) homogeneous model, (b) heterogeneous model, and (c) polyst (fat) subtraction model.

diameter 50 kV beam (N_0 spectrum from Fig. 4) incident on 5 mm diameter 5 mm thick samples. The samples were divided into 0.2 × 0.2 × 0.1 mm^3 voxels of which 7250 occupied the central ROI. The scattering was assumed to occur at the center of each voxel.[11] The Compton wavelength shift was incorporated while multiple scatter was neglected. Statistical noise was not included in the simulations. For heterogeneous samples, the materials were distributed randomly between voxels.

First, consider a sample of water. The coherent form factors from Narten[23] and the incoherent scattering functions (S) from Hubbell *et al.*[24] were used. The N_s obtained via summing over voxels in the ROI was then used in Eq. (3) to solve for μ_s of water. Figure 5(a) shows that Eq. (3) is is an effective model to extract μ_s of water.

Next, consider a heterogeneous sample consisting of polystyrene ($\nu = 0.6$), nylon (0.2), and PMMA (0.2). For the experiments this sample was a layered one, while for the simulations it was divided into voxels. The fractional volumes were (0.6, 0.2, 0.2) within both the ROI and remaining sample. The WAXS data from Ref. 22 were used. Figure 5(b) shows the $\overline{\mu}_s$ obtained using Eq. (3) with μ replaced with $\overline{\mu}$. These $\overline{\mu}_s$ values are well approximated by $\overline{\mu}_s^{\Sigma}$.

Finally, a 5 mm thick sample with ($\nu = 0.8$) water + 0.2 polyst was used to test Eq. (6). Figure 5(c) shows that $\overline{\mu}_s \approx \overline{\mu}_s^{\Sigma}$ and μ_{sc} obtained using Eq. (6) yields excellent estimates for water μ_s.

4. RESULTS AND DISCUSSIONS

Figure 6 shows μ_s signals in units of m^{-1} sr^{-1} as a function of $0.35 \leq x \leq 1.9$ nm^{-1} (bottom axis) and E (top axis) obtained for (a) polyst, (b) nylon, (c) PMMA, (d) water, and (e) fibphan. The raw spectra were binned at 0.5 keV intervals and calculations of μ_s were performed and then binned at 0.05 nm^{-1} resolution. The polyst and PMMA experiment profiles of μ_s agree with literature (dashed lines) except at the peaks where for the former a slight overshoot occurs and an undershoot for the latter. The two peaks in nylon are visible but resolution would need to be improved for better separation. The water data for $0.5 < x < 1.6$ nm^{-1} match the gold standard[23,24] and the sum 0.6 μ_s^{water} + 0.4 μ_s^{polyst} is well approximated by the fibphan measurement for the entire x range.

King and Johns[29,30] developed a method to extract μ_s from energy dispersive x-ray diffraction measurements. Their model calculations require the ratios of scatter to transmission spectra. The solid line in Fig. 6(a) was generated using their

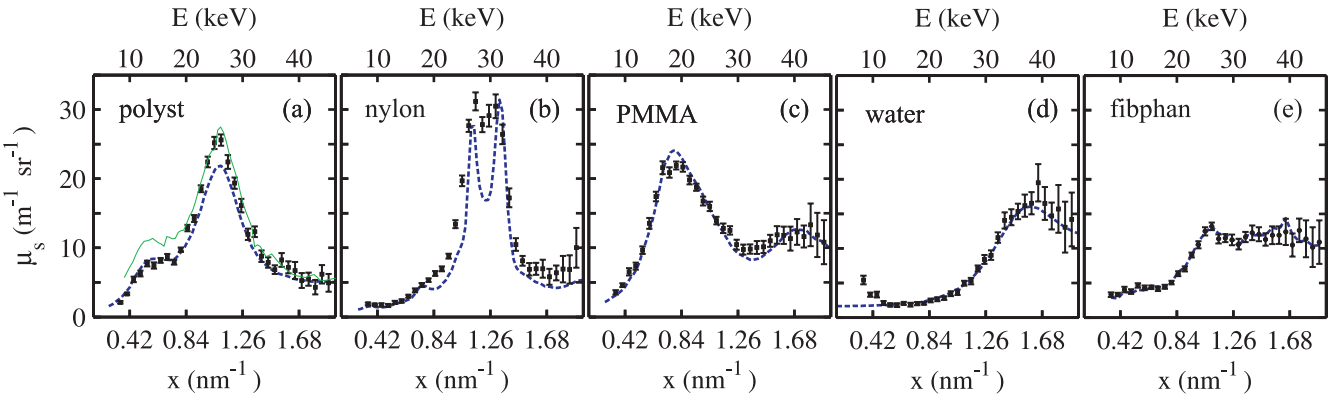

FIG. 6. μ_s for the homogeneous samples measured at $\theta = 6°$. In (a) to (c), the dashed lines were extracted from the data of Kosanetzky *et al.* (Ref. 22). The solid line in (a) was generated using F data from King *et al.* (Ref. 29), and S from Hubbell *et al.* (Ref. 24). (d) The dashed line = gold standard (Refs. 23 and 24). (e) Recall that fibphan is actually a layered two compartment sample of water and polyst (dashed line = 0.6 μ_s^{water} + 0.4 μ_s^{polyst}).

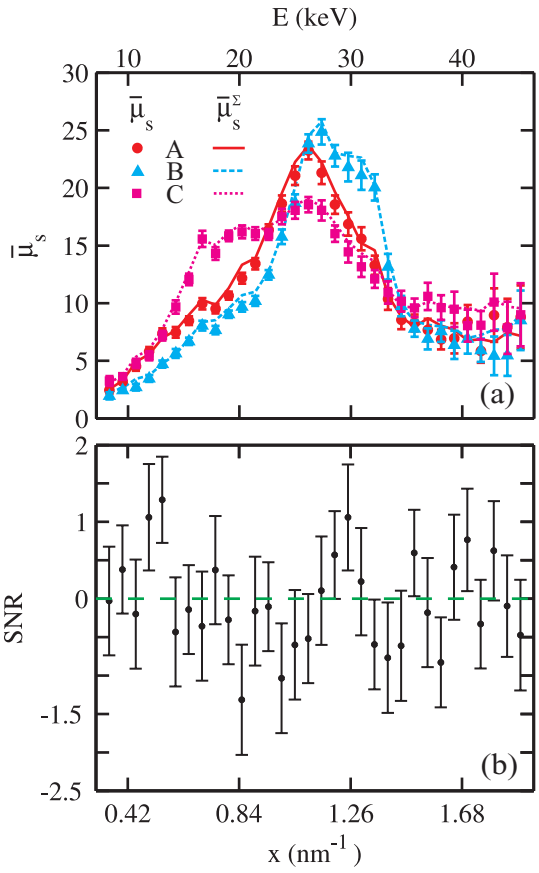

FIG. 7. (a) $\overline{\mu}_S$ for composites A = [3 mm polyst (top) + 1 mm nylon (middle) + 1 mm PMMA (bottom)], B = [1 mm polyst + 3 mm nylon + 1 mm PMMA], and C = [1 mm polyst + 1 mm nylon + 3 mm PMMA]. (b) SNR in terms of $\overline{\mu}_S$ for composite A versus A′ (a shuffled A).

F data and *S* values from Hubbell *et al.*[24] For $x < 0.8$ nm^{-1}, our measured μ_s of polyst agree with the data of Kosanetzky *et al.*[22] whereas for $x > 0.8$ nm^{-1} they are closer to the data of King *et al.*[29]

Figure 7(a) shows the $\overline{\mu}_s$ signals for composite samples with varying amounts of polyst, nylon, and PMMA. Note how $\overline{\mu}_s$ agree well with $\overline{\mu}_s^{\Sigma}$ for all samples. Figure 7(b) shows the signal-to-noise ratio (SNR) in terms of $\overline{\mu}_s$ signals between composites A (3 mm polyst + 1 mm nylon + 1 mm PMMA) and A′ (1 mm nylon + 1 mm PMMA + 3 mm polyst) a shuffled composite A. The SNR is given by

$$\mathrm{SNR} = \frac{\Delta}{\sigma_\Delta} = \frac{\overline{\mu}_{sA} - \overline{\mu}_{sA'}}{\sigma_\Delta}, \tag{7}$$

where

$$\sigma_\Delta^2 = \left(\frac{\partial \Delta}{\partial N_s^A}\right)^2 N_s^A + \left(\frac{\partial \Delta}{\partial N_s^{A'}}\right)^2 N_s^{A'} + \left(\frac{\partial \Delta}{\partial N_b}\right)^2 N_b + \left(\frac{\partial \Delta}{\partial N_s^{\mathrm{polyca}}}\right)^2 N_s^{\mathrm{polyca}} \tag{8}$$

was calculated assuming only Poisson error. The fluctuations around zero imply that ordering of compartments is not important. A t-test failed to show a statistically significant difference between $\langle \mathrm{SNR} \rangle = -0.05$ and 0, $t(31) = -0.4559$, $p < 0.05$.

Figure 8(a) shows $\overline{\mu}_s$ (dashed line) for a 4 mm water + 1 mm thick polyst composite. Upon subtraction of a 20% polyst signal, the estimates $\mu_{sc}^{\mathrm{water}}$ (circles) agree well with our measured μ_s water (solid line). For clarity, error bars were omitted for $\overline{\mu}_s$ and μ_s. Figure 8(b) shows $\overline{\mu}_s$ for a 3.33 mm fibphan + 1.67 mm polyst composite. Following a 33.4% subtraction of polyst, the data $\mu_{sc}^{\mathrm{fibphan}}$ agree with the μ_s of fibphan. Figure 8(c) shows $\mu_{sc}^{\mathrm{water}}$ estimates using the subtraction technique on other water/polyst samples. The accuracy of the subtraction method is demonstrated by the overlap of the resulting $\mu_{sc}^{\mathrm{water}}$ curves which are close to those of water. The attempt to correct for larger amounts of polyst (e.g., 80%) results in larger error bars and fluctuations.

5. CONCLUSIONS

The WAXS homogeneous model with air scatter corrections and an N_0 estimated via scattered photons provided

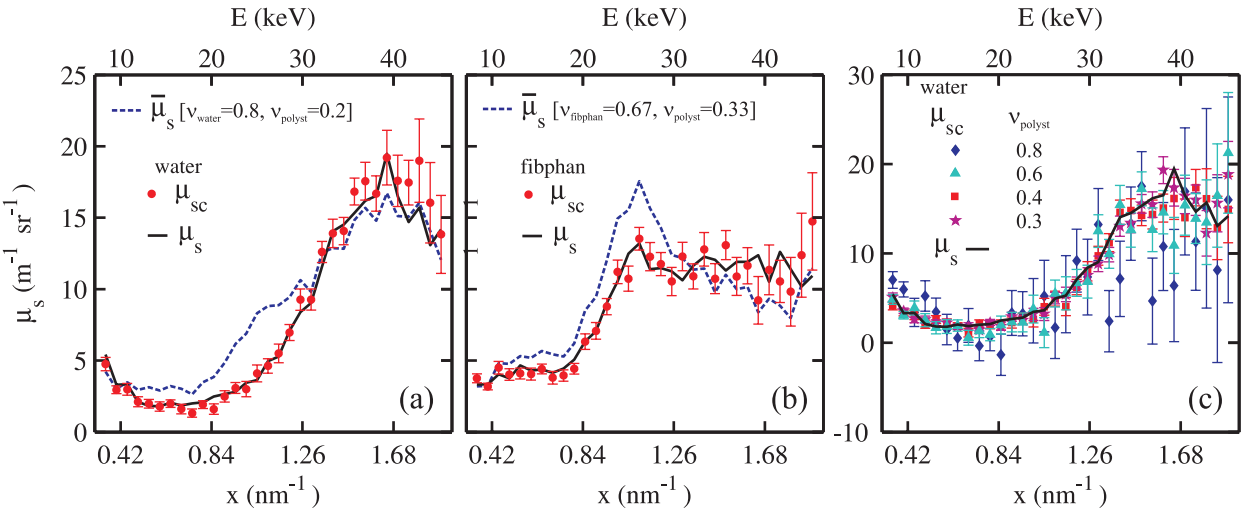

FIG. 8. Demonstration of the WAXS subtraction model. (a) $\overline{\mu}_S$ for a 4 mm water + 1 mm polyst composite and μ_{sc} for water, (b) $\overline{\mu}_S$ for a 3.33 mm fibphan + 1.67 mm polyst composite and μ_{sc} for fibphan, and (c) again for water using other water/polyst phantoms.

accurate μ_s estimates of the samples. The model predicted well the μ_s for heterogeneous biopsy phantoms. The successful subtractions of polyst (fat) signals from the composite samples were encouraging. The usefulness of the models for nonlayered biopsies were validated via the simulations. The methods can be used to compare μ_s signals of breast cancer and fibroglandular tissue without the effects of fat tissue provided one has an accurate method to estimate the volume fraction of fat. Future work will consist of devising such a method for the WAXS applications.

ACKNOWLEDGMENTS

The last author appreciated the seed funds provided by the Natural Sciences and Engineering Research Council of Canada and the Canadian Institute of Health Research-Institute of Cancer Research. Special thanks goes to Hans Schwendener, machinist with the Northeast Cancer Centre, Health Sciences North in Sudbury, for his technical and machine shop contributions.

[a]Electronic mail: rx_tang@laurentian.ca
[b]Electronic mail: cx_laamanen@laurentian.ca
[c]Electronic mail: mcdnancye@gmail.com
[d]Author to whom correspondence should be addressed. Electronic mail: rleclair@laurentian.ca

[1]S. R. Peters, *A Practical Guide to Frozen Section Technique*, 1st ed. (Springer, New York, 2010).
[2]A. Khaddage, S. Berremila, F. Forest, A. Clemenson, C. Bouteille, P. Seffert, and M. Peoc'h, "Implementation of molecular intra-operative assessment of sentinel lymph node in breast cancer," Anticancer Res. **31**, 585–590 (2011).
[3]A. L. C. Conceição, M. Antoniassi, and M. E. Poletti, "Preliminary study of human breast tissue using synchrotron radiation combining WAXS and SAXS techniques," Appl. Radiat. Isot. **68**, 799–803 (2010).
[4]A. Chaparian, M. A. Oghabian, and V. Changizi, "Introducing an optimized method for obtaining x-ray diffraction patterns of biological tissues," Iran. J. Med. Phys. **8**, 9–17 (2012).
[5]A. Chaparian, M. A. Oghabian, V. Changizi, and M. J. Farquharson, "The optimization of an energy-dispersive x-ray diffraction system for potential clinical application," Appl. Radiat. Isot. **68**, 2237–2245 (2010).
[6]W. M. Elshemey, O. S. Desouky, M. M. Fekry, S. M. Talaat, and A. A. Elsayed, "The diagnostic capability of x-ray scattering parameters for the characterization of breast cancer," Med. Phys. **37**, 4257–4265 (2010).
[7]S. Pani, E. J. Cook, J. A. Horrocks, J. L. Jones, and R. D. Speller, "Characterization of breast tissue using energy-dispersive x-ray diffraction computed tomography," Appl. Radiat. Isot. **68**, 1980–1987 (2010).
[8]V. Changizi, A. A. Kheradmand, and M. A. Oghabian, "Application of small-angle x-ray scattering for differentiation among breast tumors," J. Med. Phys. **33**, 19–23 (2008).
[9]J. A. Griffiths, G. J. Royle, A. M. Hanby, J. A. Horrocks, S. E. Bohndiek, and R. D. Speller, "Correlation of energy dispersive diffraction signatures and microCT of small breast tissue samples with pathological analysis," Phys. Med. Biol. **52**, 6151–6164 (2007).
[10]E. A. Ryan and M. J. Farquharson, "Breast tissue classification using x-ray scattering measurements and multivariate data analysis," Phys. Med. Biol. **52**, 6679–6696 (2007).
[11]R. J. LeClair, M. M. Boileau, and Y. Wang, "A semianalytic model to extract differential linear scattering coefficients of breast tissue from energy dispersive x-ray diffraction measurements," Med. Phys. **33**, 959–967 (2006).
[12]G. Kidane, R. D. Speller, G. J. Royle, and A. M. Hanby, "X-ray scatter signatures for normal and neoplastic breast tissues," Phys. Med. Biol. **44**, 1791–1802 (1999).
[13]M. Yaffe, "Mammographic density. Measurement of mammographic density," Breast Cancer Res. **10**, 209 (2008).
[14]R. J. LeClair and P. C. Johns, "X-ray forward-scatter imaging: Experimental validation of model," Med. Phys. **28**, 210–219 (2001).
[15]R. J. LeClair and P. C. Johns, "A semianalytic model to investigate the potential applications of x-ray scatter imaging," Med. Phys. **25**, 1008–1020 (1998).
[16]R. J. LeClair and P. C. Johns, "Optimum momentum transfer arguments for x-ray forward scatter imaging," Med. Phys. **29**, 2881–2890 (2002).
[17]R. J. LeClair and P. C. Johns, "Analysis of spectral blur effects in x-ray scatter imaging," Med. Phys. **26**, 1811–1816 (1999).
[18]D. R. White, "Tissue substitutes in experimental radiation physics," Med. Phys. **5**, 467–479 (1978).
[19]B. Alberts, A. Johnson, J. Lewis, M. Raff, K. Roberts, and P. Walter, *Molecular Biology of the Cell*, 5th ed. (Garland Science, New York, 2008).
[20]O. O. Mykhaylyk and C. M. Martin, "Effect of unsaturated acyl chains on structural transformations in triacylglycerols," Eur. J. Lipid Sci. Technol. **111**, 227–235 (2009).
[21]S. Krimm and A. V. Tobolsky, "Quantitative x-ray studies of order in amorphous and crystalline polymers: Scattering from various polymers and a study of the glass transition in polystyrene and polymethyl methacrylate," Text. Res. J. **21**, 805–822 (1951).
[22]J. Kosanetzky, B. Knoerr, G. Harding, and U. Neitzel, "X-ray diffraction measurements of some plastic materials and body tissues," Med. Phys. **14**, 526–532 (1987).
[23]A. H. Narten, "X-ray diffraction data on liquid water in the temperature range 4 °C–200 °C," Oak Ridge National Laboratory Report No. ORNL 4578, 1970.
[24]J. H. Hubbell, Wm. J. Veigele, E. A. Briggs, R. T. Brown, D. T. Cromer, and R. J. Howerton, "Atomic form factors, incoherent scattering functions, and photon scattering cross sections," J. Phys. Chem. Ref. Data **4**, 471–538 (1975); Erratum, **6**, 615–616(E) (1977).
[25]E. F. Plechaty, D. E. Cullen, and R. J. Howerton, "Tables and graphs of photon interaction cross sections from 1.0 keV to 100 MeV derived from the LLL evaluated nuclear data library," UCRL-50400, Vol. 6, Revision 1, Lawrence Livermore Laboratory (1975).
[26]P. C. Johns and M. J. Yaffe, "X-ray characterization of normal and neoplastic breast tissues," Phys. Med. Biol. **32**, 675–695 (1987).
[27]R. J. LeClair, Y. Wang, P. Zhao, M. Boileau, L. Wang, and F. Fleurot, "An analytic model for the response of a CZT detector in diagnostic energy dispersive x-ray spectroscopy," Med. Phys. **33**, 1329–1337 (2006).
[28]M. Yaffe, K. W. Taylor, and H. E. Johns, "Spectroscopy of diagnostic x rays by a compton-scatter method," Med. Phys. **3**, 328–334 (1976).
[29]B. W. King, K. A. Landheer, and P. C. Johns, "X-ray coherent scattering form factors of tissues, water and plastics using energy dispersion," Phys. Med. Biol. **56**, 4377–4397 (2011).
[30]B. W. King and P. C. Johns, "An energy-dispersive technique to measure x-ray coherent scattering form factors of amorphous materials," Phys. Med. Biol. **55**, 855–871 (2010).